ANNUAL REVIEWS

Annual Review of Fluid Mechanics

Symmetry-Breaking Cilia-Driven Flow in Embryogenesis

David J. Smith,[1,2] Thomas D. Montenegro-Johnson,[1] and Susana S. Lopes[3]

[1]School of Mathematics, University of Birmingham, Edgbaston, Birmingham B15 2TT, United Kingdom; email: d.j.smith@bham.ac.uk

[2]Institute of Metabolism and Systems Research, University of Birmingham, Edgbaston, Birmingham B15 2TT, United Kingdom

[3]Chronic Diseases Research Centre (CEDOC), NOVA Medical School Faculdade de Ciências Médicas, Universidade Nova de Lisboa, 1169-056 Lisboa, Portugal

Annu. Rev. Fluid Mech. 2019. 51:105–28

First published as a Review in Advance on August 15, 2018

The *Annual Review of Fluid Mechanics* is online at fluid.annualreviews.org

https://doi.org/10.1146/annurev-fluid-010518-040231

Keywords

body axis determination, cilia, nodal flow, ventral node, Kupffer's vesicle

Abstract

The systematic breaking of left–right body symmetry is a familiar feature of human physiology. In humans and many animals, this process originates with asymmetric fluid flow driven by rotating cilia, occurring in a short-lived embryonic organizing structure termed the node. The very low–Reynolds number fluid mechanics of this system is reviewed; important features include how cilia rotation combines with tilt to produce asymmetric flow, boundary effects, time dependence, and the interpretation of particle tracking experiments. The effect of perturbing cilia length and number is discussed and compared in mouse and zebrafish. Whereas understanding of this process has advanced significantly over the past two decades, there is still no consensus on how flow is converted to asymmetric gene expression, with most research focusing on resolving mechanical versus morphogen sensing. The underlying process may be more subtle, probably involving a combination of these effects, with fluid mechanics playing a central role.

1. INTRODUCTION

The systematic left–right asymmetry of the interior of the human body is familiar to all of us; unless an individual has the rare condition situs inversus, the heartbeat is clearly palpable on the left side of the chest (**Figure 1*a***). The left–right axis is the last to form in the developing embryo, following the establishment of the anterior–posterior (head–tail) and dorsal–ventral (back–front) axes (Hirokawa et al. 2009); if left–right symmetry breaking were random, one would expect to see 50% of the population with their heart on the right—why is this not the case?

As is now well established in developmental biology, the answer lies with cilia-driven fluid flow taking place early in development. This flow is the first left–right asymmetric event and occurs in a short-lived embryonic cavity or organizing structure such as the primitive node in humans (Schoenwolf et al. 2014), ventral node of mouse (**Figure 1*b***) (Nonaka et al. 1998) and rabbit (Okada et al. 2005), and Kupffer's vesicle (KV) of medakafish (Okada et al. 2005) and zebrafish (Essner et al. 2005, Kramer-Zucker et al. 2005) [the story in the chick embryo is however different (see Levin et al. 1995, Gros et al. 2009)]. Ten years ago, a landmark review in this journal (Hirokawa et al. 2009) summarized the rapid progress in the period from 1998 to 2009 in which the following findings were established. (*a*) The ventral node of the mouse, and analogous structures in most (Nonaka et al. 1998, 2002; Essner et al. 2005; Kramer-Zucker et al. 2005; Schweickert et al. 2007) but not quite all (Gros et al. 2009) model organisms, is the initial location of left–right asymmetric directional flow. (*b*) The flow is driven by a sparse (one-per-cell) population of cilia, which rotate clockwise (viewed from tip to base); loss of cilia in mutant embryos results in loss of flow and randomized asymmetry. (*c*) This flow produces left–right asymmetric gene expression in the node, which subsequently spreads to the rest of the lateral plate mesoderm—sheets of embryonic tissue at the left and right edges of the embryo that subsequently contribute to the circulatory system and body wall (Nonaka et al. 1998). (*d*) Tilt of the cilia toward an already established axis combines with rotational chirality to produce left–right asymmetric fluid dynamics (Cartwright et al. 2004, Okada et al. 2005, Nonaka et al. 2005). A visual summary of the process is shown in **Figure 1*c–f***.

These developments in biology were accompanied by a series of theoretical and computational studies that further elucidated the essential fluid mechanics of flow generation (Brokaw 2005; Buceta et al. 2005; Cartwright et al. 2007; Smith et al. 2007, 2008). The excitement and rapid progress during that decade can be appreciated by retracing the long pathway by which the role of cilia in left–right symmetry breaking was gradually uncovered. Readers are referred to, for example, Siewert and Kartagener's work on the triad syndrome in the early twentieth century (reviewed in Berdon & Willi 2004 and Berdon et al. 2004), the discovery of the *inversus viscerum* (*iv*/*iv*) mouse (Hummel & Chapman 1959), the postulate that motile embryonic cilia are instrumental in determining situs (Afzelius 1976), the puzzle regarding motility of *iv*/*iv* cilia (Handel & Kennedy 1984), the study of the ventral node of mouse and the discovery of motile cilia (Sulik et al. 1994), further debate over the motility of nodal cilia (Supp et al. 1997), and the final confirmation of the necessary (Nonaka et al. 1998) and sufficient (Nonaka et al. 2002) role of cilia-driven flow in determining situs.

The final major question concerned the conversion of asymmetric directional flow to the earliest asymmetric gene expression [initially, the earliest asymmetry was thought to involve *Nodal* on the left edge of the node in mouse; subsequent work has shown that rightward elevation of *Cerl2* occurs earlier in *Xenopus* (Schweickert et al. 2010), zebrafish (Lopes et al. 2010), and mouse (Shinohara et al. 2012)]. Two major early hypotheses emerged: (*a*) nodal flow creates a left–right gradient of a morphogen (chemosensing) (Nonaka et al. 1998, Okada et al. 2005), and (*b*) nodal flow is sensed mechanically by immotile cilia at the periphery, leading to asymmetric calcium signaling (mechanosensing) (McGrath et al. 2003). The morphogen hypothesis was further elaborated by

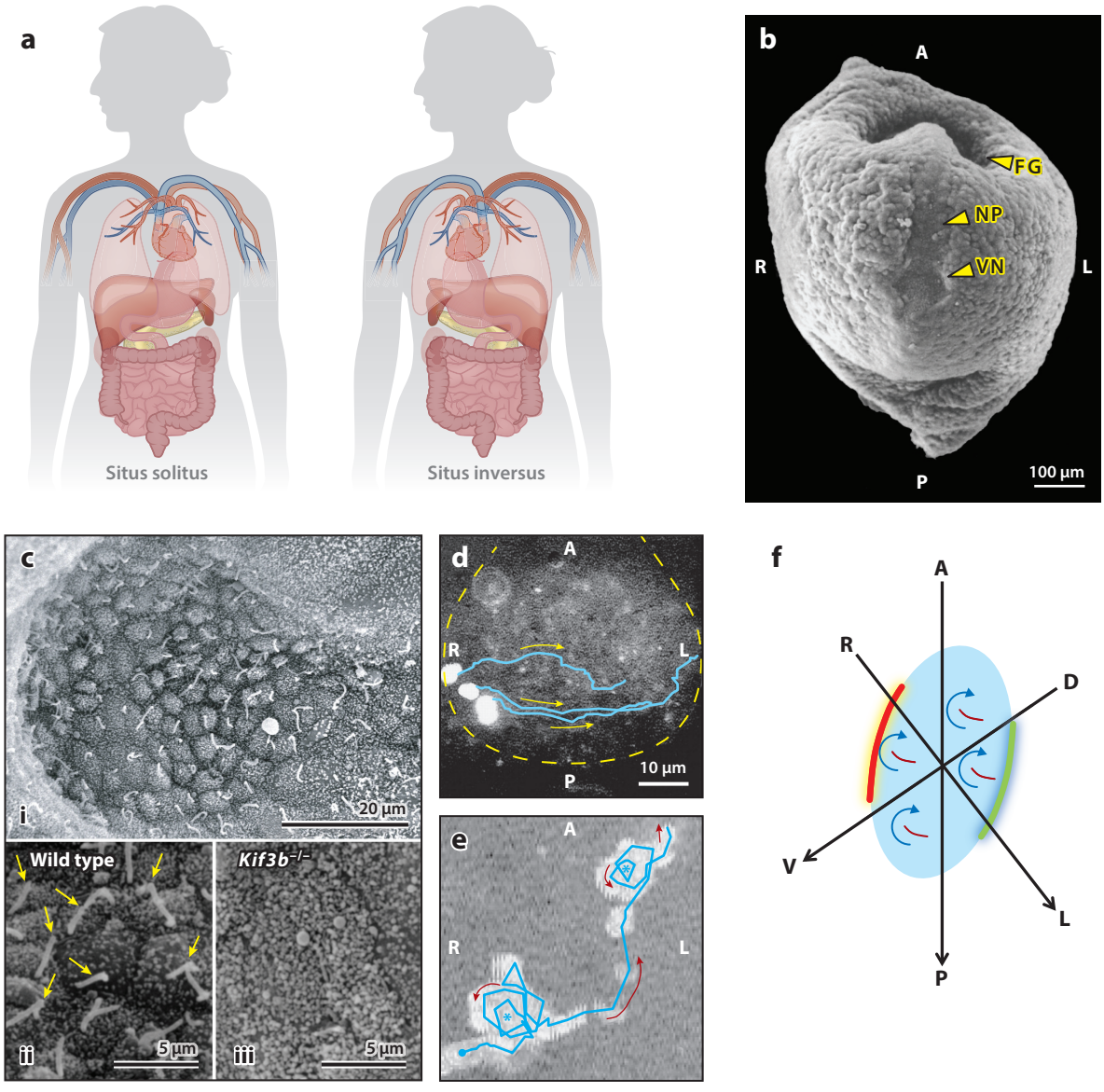

Figure 1

The left–right asymmetric body plan originates with cilia-driven flow early in development. (*a*) Schematic drawing showing normal (situs solitus) and reversed (situs inversus) placement of the heart and liver in humans. Panel *a* adapted from Hirokawa et al. (2009). (*b*) Electron micrograph of the ventral side of a mouse embryo at 7.5 days post coitus. (*c*) Electron micrograph of the ventral node of the mouse showing cilia (*i*), along with close-ups showing cilia (*yellow arrows*) in wild-type mice (*ii*) and the absence of cilia in *Kif3b*$^{-/-}$ mutant mice with deficient intraflagellar transport (*iii*). Panel *b* and subpanel *i* of panel *c* adapted with permission from from Hirokawa et al. (2006), copyright 2006 Elsevier. (*d*) Leftward transport of material in the node by cilia-driven flow. (*e*) Close-up showing detail of particle tracks, including apparent trapping and release by cilia (embryonic left is shown on the right of the image). Panels *d* and *e* and subpanels *ii* and *iii* of panel *c* adapted with permission from Nonaka et al. (1998), copyright 1998 Elsevier. (*f*) Schematic showing the body axes in relation to the node, with asymmetric gene expression illustrated with red and green lines. Abbreviations: A, anterior; D, dorsal; FG, foregut; L, left; NP, notochordal plate; P, posterior; R, right; V, ventral; VN, ventral node.

the discovery of morphogen-containing vesicles termed nodal vesicular parcels (NVPs) (Tanaka et al. 2005). Hirokawa et al. (2009) concluded that the problem of the origin of left–right symmetry breaking was essentially solved, the discovery of NVPs being the final piece of the puzzle.

However, in the intervening years a consensus has still not been reached. Shinohara et al. (2012) made the remarkable observation that mutant embryos with only two motile cilia produce consistently elevated *Cerl2* expression on the right, despite very weak and localized flow. Moreover, even in normal embryos, asymmetric expression of *Cerl2* occurred in the early stages of cilia-driven flow, before a global flow was established. These observations were interpreted as supporting mechanosensing rather than a transport-based process. By contrast, through imaging of live cells from a transgenic mouse model expressing a ratiometric genetically encoded calcium indicator, Delling et al. (2016) reported that nodal cilia are not calcium-sensitive sensors. These experimental observations, combined with further imaging and modeling of the fluid mechanics of the organizing structures that we review in detail below, have revealed hitherto unexpected subtlety in the process of left–right symmetry breaking. This review summarizes the advances of the last ten years of interdisciplinary research that links fluid mechanics to physiological and biomolecular processes. It is argued that an integrative approach will be essential to reveal the secrets of the node.

2. MATHEMATICAL, PHYSICAL, AND LIVING MODELS OF NODAL FLOW

Mathematically oriented fluid mechanicians and physicists most commonly formulate models as differential equations and initial/boundary conditions to be solved, analyzed, or approximated (Cartwright et al. 2004, Smith et al. 2007); computational scientists may interpret a model as a computer simulation, a subtly different scientific viewpoint that often involves similar methods—in particular, the use of extensive computer calculations (Buceta et al. 2005, Sampaio et al. 2014, Chen & Zhong 2015). Another overlapping concept is a model of the three-dimensional (3D) geometry and motion, which is essential to formulating a mechanical understanding of a system but also of interest in its own right (Smith et al. 2012). Experimental fluid mechanicians may interpret a model as a physical construction built in the laboratory (Nonaka et al. 2005). By contrast, biological and biomedical scientists refer to animal models of human development and human disease, as exemplified by the use of mouse (both wild-type and mutant strains), rabbit, *Xenopus*, zebrafish, and medakafish as animal models of embryo development (Blum et al. 2014). Finally, scientists of all backgrounds have their own conceptual models of the functioning of their system of interest—in terms of physical, biomolecular, and physiological processes. We review recent advances involving all of the above types of model, often in combination, but with a focus on accurate fluid mechanical understanding. Details of the molecular biology of the left–right pathway are beyond the scope of this article except where they directly affect mechanical parameters such as cilia length and motility; therefore, the reader is referred to recent reviews by Shinohara & Hamada (2017) and Schweickert et al. (2018).

2.1. Conceptual Models of Symmetry-Breaking by Flow

Figure 2 summarizes the main conceptual models in the biological literature of how cilia-driven flow is produced and converted to asymmetric gene expression in the mouse. Cells on the floor of the ventral node express a single motile primary cilium (Nonaka et al. 1998), the base of which is shifted toward the posterior of the curved surface of the cell (Hashimoto et al. 2010), producing a posterior tilt (Okada et al. 2005). Cilia rotate clockwise, viewed tip-to-base, at about

10 Hz. Because cilia are tilted, they are relatively upright during the leftward portion of the beat cycle and relatively close to the cell surface during the rightward portion; the viscous resistance associated with the cell surface results in greater leftward transport (Brokaw 2005, Nonaka et al. 2005, Okada et al. 2005), as shown in **Figure 2*a***. The resulting leftward particle transport is often termed "unidirectional flow" in the literature (see for example Hirokawa et al. 2009, Yoshiba et al. 2012, Chen & Zhong 2015, Pennekamp et al. 2015).

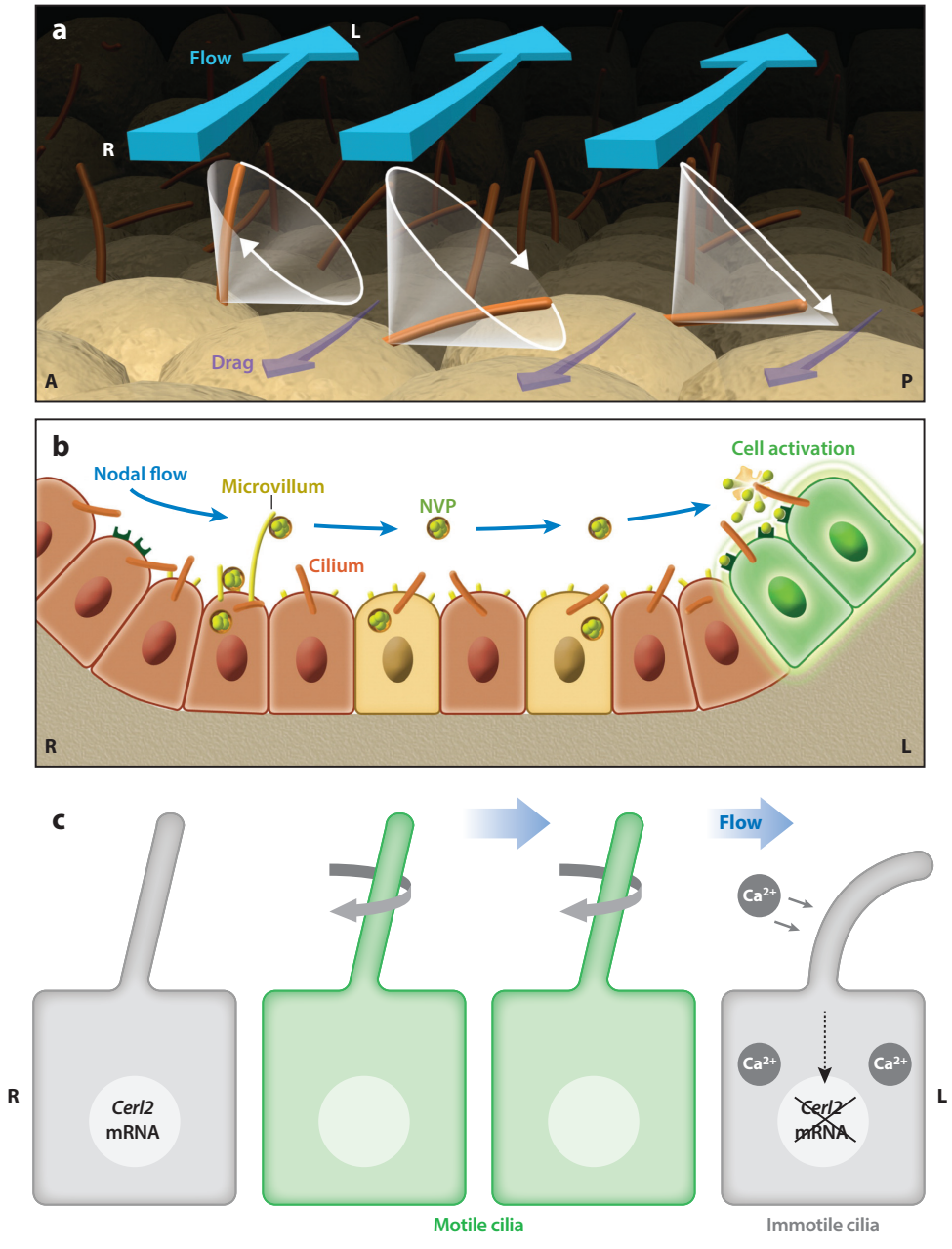

(Caption appears on following page)

Figure 2 (*Figure appears on preceding page*)

Conceptual models of flow generation and conversion. (*a*) Rotating cilia, positioned toward the posterior of the curved cell surface and hence tilted posteriorly, drive an effective flow when moving to the left, followed by a flow that is less effective when moving to the right due to hydrodynamic resistance of the cell surface. (*b*) The nodal vesicular parcel (NVP) theory of flow conversion. Vesicles containing morphogens are extruded into the fluid and swept toward the left (depicted on the right-hand side) by motile cilia in the interior of the node; these particles reach the left-hand periphery of the node, where they are then broken up by cilia, releasing morphogens and hence causing secondary intracellular signals. Panels *a* and *b* adapted with permission from Hirokawa et al. (2006), copyright 2006 Elsevier. (*c*) The mechanosensing or two-cilia theory of flow conversion. Motile cilia in the interior sweep fluid to the left, causing immotile peripheral cilia to bend, inducing a calcium ion signal. Panel *c* adapted from Hirokawa et al. (2009). Abbreviations: A, anterior; L, left; mRNA, messenger RNA; P, posterior; R, right.

The fluid dynamic picture in the node of the rabbit embryo, and KV of medakafish, appears to be similar to the mouse (Okada et al. 2005): One ciliated surface produces a consistent directional flow. KV of zebrafish is also intensively studied; however, this system is geometrically and fluid dynamically more complicated because cilia protrude from cells on all internal surfaces of the cavity (with spatially varying density), and the tilt direction may not be uniform (Kreiling et al. 2007, Supatto et al. 2008, Ferreira et al. 2017). Moreover, the system produces left–right asymmetry less consistently in wild type, and it is less robust to perturbations in cilia number (Sampaio et al. 2014, Smith et al. 2014); we focus on the KV system of zebrafish in Section 2.3.

The next issue to resolve is flow conversion, i.e., how the asymmetric fluid dynamics is perceived (Norris 2012) by the cells of the node and converted to asymmetric gene expression. The initial hypothesis advanced by Nonaka et al. (1998) was that cilia-driven flow could produce a gradient of dissolved morphogens; indeed, subsequent experiments with fluorescent proteins (Okada et al. 2005) established that in the embryo culture setting with removed upper membrane, nodal flow can produce a leftward concentration bias of proteins in the approximate range of 15–50 kDa, measured 60 s after release of the fluorescent proteins. However, there are two complications with the applicability of the dissolved morphogen model in vivo. First, Nonaka et al.'s (2002) artificial flow reversal experiment showed that unphysiologically fast flow (110 μm/s) could reverse situs in wild-type embryos. The fast flow regime in an open cavity seems likely to wash away secreted morphogens, so there must be an alternative mechanism in place to explain the observations. This interpretation has been contested (Okada et al. 2005); however, it is clear that fast flow experiments produce very different morphogen concentrations than slow physiological flow. The second complication concerning the dissolved morphogen model is that the concentration difference in Okada et al.'s experiments did not reach steady state during the 100 s course—the enclosed nature of the physiological node and associated upper deck return flow (discussed below) seem highly likely to produce a uniform concentration of morphogen across the node over a timescale of minutes. Indeed, Cartwright et al. (2004) calculated vertical diffusion timescales of 0.25–2.5 s and left–right advection timescales of 1–5 s in wild type, proposing that any putative left–right asymmetric morphogen must be subject to a process of inactivation on a shorter timescale for this mechanism to be viable.

The NVP model advanced by Tanaka et al. (2005) (**Figure 2*b***) appeared to resolve these difficulties with the morphogen model, providing a mechanism by which morphogens could be delivered asymmetrically. It was proposed that NVPs carrying a payload of the morphogens Sonic hedgehog and retinoic acid are extruded from the nodal pit cells by microvilli. These NVPs are transported to the left by the rotating cilia, whereupon they are broken up by cilia at the edge, releasing their cargo in the correct location. This model formed the focus of the review by Hirokawa et al. (2009).

Okada et al. (1999) discussed mechanical sensing as a theoretical alternative to morphogen sensing; this idea was discussed more seriously by Brueckner (2001), who suggested that cilia at the edge of the node could be a candidate sensor for flow. The observation of calcium signaling at the edge of the node, combined with the discovery that a cation channel is necessary for left–right determination (McGrath et al. 2003), led to the proposal of a mechanosensing model of flow conversion, also called the two cilia model (Tabin & Vogan 2003). As depicted in **Figure 2*c***, leftward flow generated by cilia causes bending of immotile cilia located to the left; this bending produces a cellular calcium signal, which induces secondary messengers. More recent evidence both for and against both the NVP hypothesis and the mechanosensing hypothesis is reviewed in Section 5.1. We now turn to exploring the fluid mechanics of nodal flow.

2.2. Fluid Mechanical Models of Cilia-Driven Flow

The basis for mathematical modeling of cilia-driven flow is the observation that the Reynolds number, which quantifies the relative importance of inertial to viscous effects, is much smaller than one: Taking a typical cilium length of 5 μm and rotational frequency of 10 Hz, the Reynolds number for flow produced by a cilium is less than 0.002. This places the flow firmly within the Stokes flow regime, in which viscous effects dominate inertia, even if the extraembryonic fluid has a low viscosity (i.e., similar to saline). Consequences of the inertialess regime include (*a*) the fact that the flow is instantaneously determined by its forcing, so that when a cilium is performing the leftward part of its stroke, it drives the surrounding fluid to the left, but when it is performing the rightward part of its stroke, it drives the surrounding fluid to the right. Time-averaged transport is only produced because the leftward and rightward motions differ in effectiveness. (*b*) Boundaries such as the floor of the node and the overlying membrane have important consequences for the nature of the flow away from the immediate envelope of the cilium, including inducing more rapid decay of cilium forcing. (*c*) Intuitions from day-to-day fluid mechanical effects such as the streaming flow produced by rotating propellers are misleading; in particular, the flow produced by a localized force is symmetric from front to back.

The other key physical effect in the system is Brownian motion, the continuous random displacement of particles of approximately micron size and smaller. The NVPs reported by Tanaka et al. (2005) and indeed any flow tracer—for example, the native debris imaged by Nonaka et al. (1998), Supatto et al. (2008), and Sampaio et al. (2014) and the fluorescent 0.2-μm-diameter microbeads used for particle imaging velocimetry (PIV) by Shinohara et al. (2012)—are subject to significant Brownian effects. From the Stokes–Einstein relation, the Brownian diffusion coefficient of such a bead can be estimated to be approximately 2 $\mu m^2/s$. The size range reported for NVPs is quite broad (about 0.1–2.5 μm); Brownian effects are important throughout most of this range. The implications are that (*a*) morphogen-containing vesicles do not behave as Lagrangian tracers (i.e., they do not faithfully follow the fluid velocity field), and (*b*) experimental measurements of flow based on imaging small particles—in particular, PIV—must be carried out via cross-correlation over extended time windows corresponding to tens to hundreds of beat cycles. It is therefore not possible to measure the time-varying flow field instantaneously via imaging of either submicron tracers or native vesicles.

The mathematical formulation begins with the dimensionless Stokes flow equations,

$$-\nabla p + \mu \nabla^2 \mathbf{u} = \mathbf{0} \quad \text{and} \quad \nabla \cdot \mathbf{u} = 0, \qquad 1.$$

where μ is dynamic viscosity, p is pressure, and $\mathbf{u} = \mathbf{u}(\mathbf{x}, t)$ is fluid velocity. The lack of a time derivative in these equations corresponds to the lack of inertia. The linearity of these equations

provides the basis for mathematical/computational models based on techniques such as singularity distributions, boundary integral methods, and regularized Stokeslet methods.

It was initially unclear how rotating cilia could create purely leftward particle transport; the initial explanation suggested by Nonaka et al. (1998) centered on the triangular shape of the node potentially amplifying leftward motion over rightward. The first—and perhaps most significant—theoretical advance came with the work of Cartwright et al. (2004). The earliest observations of nodal flow uncovered that (*a*) cilia perform a clockwise rotational motion (viewed tip-to-base) and (*b*) the flow generates a leftward particle transport (**Figure 1*d–f***). However, the physics by which cilia rotation causes leftward particle transport without the left–right asymmetry being already present was unclear. Cartwright et al. (2004) made the theoretical prediction that if cilia were tilted toward the already established posterior axis, then the flow above the cilia tips would be directed toward the left. This prediction was modeled mathematically by approximating the effect of each cilium via the rotlet solution of the Stokes flow Equation 1, which physically represents the flow due to a localized rotation and can be derived as the antisymmetric part of a Stokes doublet [the first derivative of the Stokeslet; see Equation 4 below and Blake & Chwang (1974)]. The steady fluid velocity $\mathbf{u}(\mathbf{x})$ given by a rotlet of strength $\mathbf{L}$ located at $\mathbf{y}$ is given by

$$\mathbf{u}(\mathbf{x}) = \frac{1}{8\pi |\mathbf{x}-\mathbf{y}|^3}\mathbf{L} \times (\mathbf{x}-\mathbf{y}). \qquad 2.$$

The flow velocity due to an array of untilted cilia, followed by tilted cilia, was investigated. As may be expected, the untilted cilia produced only a vortical flow, whereas the tilted cilia produced continuous layers of leftward flow above the rotlets (corresponding to the true flow domain) and rightward flow below the rotlets (effectively, beneath the node floor). This prediction was soon confirmed experimentally by Okada et al. (2005) and Nonaka et al. (2005); both groups observed elliptical paths of the cilia tips, indicating that the cilium traces out a tilted cone, as shown in **Figure 3*c***. Moving from theoretical to experimental fluid dynamics models, Nonaka et al. (2005) implemented an experimental realization of transport of viscous fluid via conical rotation by actuating a 6-mm wire in a highly viscous fluid, ensuring that the very low–Reynolds number Stokes flow regime was recaptured. Particle transport was quantified by adding glitter particles to the fluid; it was observed that a semicone angle of 60° and tilt angle of 30° produced greater flow transport than a semicone angle of 45° and tilt angle of 45°. We return to this observation shortly. It is of interest that in the more general setting of elastohydrodynamic modeling, a tilted rotational motion has been found to be energetically optimal in certain regions of parameter space; as the viscosity increases relative to elastic stiffness, the optimal beat pattern becomes more planar (Eloy & Lauga 2012).

Cartwright et al.'s (2004) study is an excellent example of a true theoretical prediction, as opposed to a retrodiction, and in a geometric sense captured the essence of the system. The next step was to take into account the fundamental fluid dynamical effects present, in particular, the effect of the cell surface boundary from which the cilia project. Equation 1 is augmented by the no-slip, no-penetration condition, $\mathbf{u}(\mathbf{X}, t) = \dot{\mathbf{X}}$, for all points $\mathbf{X}$ belonging to a solid surface bounding or immersed in the fluid, where the dot denotes the material time derivative. This constraint manifests as a surface stress that acts on the fluid, qualitatively and quantitatively changing the flow field.

Great physical insight into the effect of boundaries can be gained by studying the fundamental solution of the Stokes flow equations; this solution also forms the basis for many efficient and accurate mathematical and computational models. Consider the Stokes flow equations with singular forcing,

$$-\nabla p + \mu\nabla^2\mathbf{u} + \delta(\mathbf{x}-\mathbf{y})\mathbf{e}_k = 0 \quad \text{and} \quad \nabla \cdot \mathbf{u} = 0, \qquad 3.$$

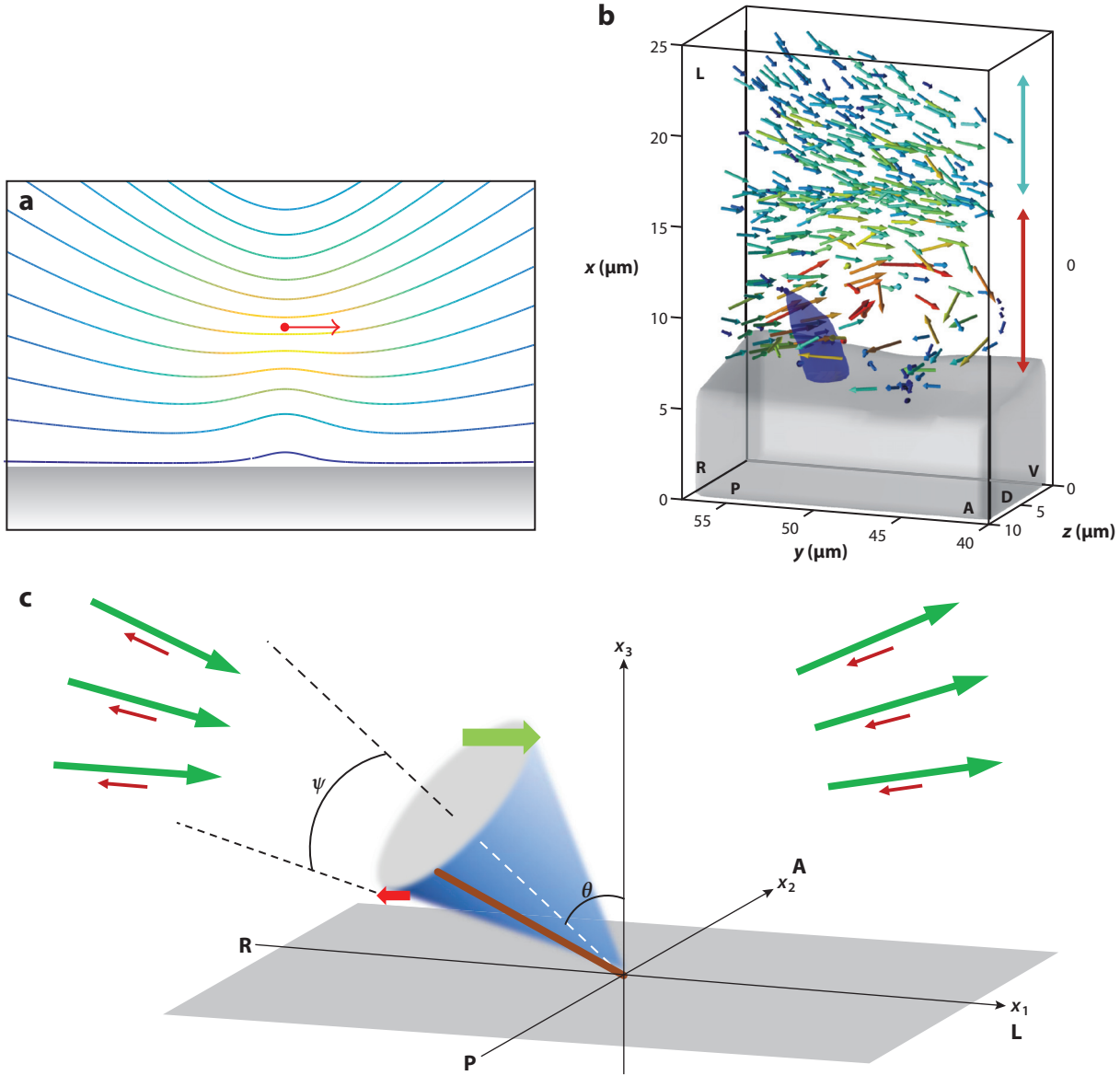

Figure 3

The fluid dynamical effect of the cell surface boundary. (*a*) Streamlines of a blakelet, i.e., a localized force acting near a plane surface; note the radial nature of the streamlines in the far field (*extreme left and right*). (*b*) Experimental data from Supatto et al. (2008) showing near-field rotational flow and far-field directional flow in the zebrafish embryo. Panel *b* adapted with permission from Supatto et al. (2008), copyright 2008 Elsevier. (*c*) Schematic of the conical model of a rotating cilium, with tilt angle θ and semicone angle ψ; green arrows show the effect of the leftward phase of the cilium stroke, and red arrows show the less-effective rightward phase. The arrows are drawn to indicate the stresslet nature of the far field. Panel *c* redrawn from Smith et al. (2012). Abbreviations: A, anterior; D, dorsal; L, left; P, posterior; R, right; V, ventral.

where $\delta(\mathbf{x}-\mathbf{y})$ denotes a Dirac delta function around the point $\mathbf{y}$ and $\mathbf{e}_k$ is a unit vector pointing in the k direction. This equation represents flow driven by a unit force, with infinitely concentrated force per unit volume; equivalently, it can be viewed as a far-field approximation to flow driven by a sphere of radius a in the limit as a approaches 0 with Stokes drag, $6\pi a\mu U = 1$, held constant. The velocity part of the solution to Equation 3 is given by

$$u_j(\mathbf{x}) = \frac{1}{8\pi\mu}\left[\frac{\delta_{jk}}{|\mathbf{x}-\mathbf{y}|} + \frac{(x_j-y_j)(x_k-y_k)}{|\mathbf{x}-\mathbf{y}|^3}\right] := S_{jk}(\mathbf{x},\mathbf{y}), \qquad 4.$$

where the right-hand side is termed the Oseen tensor, after C.W. Oseen, or the Stokeslet (a term coined by G.J. Hancock). The linearity of the Stokes flow equations entails that solutions may be constructed from point distributions, line and surface integrals of the Stokeslet, and indeed its derivatives as well.

The boundary integral method for Stokes flow (Pozrikidis 1992) is based on the idea of replacing the boundary with surface distributions of Stokeslets. One way to interpret the effect of a boundary surface therefore is to notice that the far-field decay of the Stokeslet is as $1/r$, where $r = |\mathbf{x}-\mathbf{y}|$. This slow decay implies that boundaries have long-range effects. In more precise terms, one can consider Equation 3 in the vicinity of a plane no-slip boundary, $x_3 = 0$, on which the condition $\mathbf{u} = 0$ is required to hold. This problem may be solved by the method of images, as developed by Blake (1971) for the problem of modeling ciliated protozoa. The form of the solution is $u_j = B_{jk}$, where we have

$$\begin{aligned} B_{jk}(\mathbf{x},\mathbf{y}) = \frac{1}{8\pi\mu}\Bigg\{&\left[\frac{\delta_{jk}}{r} + \frac{r_j r_k}{r^3}\right] - \left[\frac{\delta_{jk}}{R} + \frac{R_j R_k}{R^3}\right] \\ &+ 2y_3(\delta_{k\alpha}\delta_{\alpha l} - \delta_{k3}\delta_{3l})\frac{\partial}{\partial R_l}\left[\frac{y_3 R_j}{R^3} - \left(\frac{\delta_{j3}}{R} + \frac{R_j R_3}{R^3}\right)\right]\Bigg\}, \end{aligned} \qquad 5.$$

α equals 1 or 2, and r and R are defined as follows,

$$\begin{aligned} r &= [(x_1-y_1)^2 + (x_2-y_2)^2 + (x_3-y_3)^2]^{\frac{1}{2}} \\ \text{and} \quad R &= [(x_1-y_1)^2 + (x_2-y_2)^2 + (x_3+y_3)^2]^{\frac{1}{2}}, \end{aligned} \qquad 6.$$

the variables r_i and R_i being apparent from these definitions. The term $(\delta_{k\alpha}\delta_{\alpha l} - \delta_{k3}\delta_{3l})$ is simply 1 if $j = k = 1, 2$ and -1 if $j = k = 3$; the derivative term on the second line corresponds to a source dipole and a Stokes doublet. This solution has been termed the blakelet (Smith 2018).

The image system radically changes the far field associated with the Stokeslet: The far field of the flow induced by a localized force acting parallel to a plane no-slip boundary takes the form of a symmetric Stokes doublet or stresslet,

$$S_{i\alpha} \sim \frac{3}{2\pi\mu}\frac{r_i r_\alpha r_3}{r^5}, \qquad 7.$$

which decays as $1/r^2$ and produces radial streamlines (**Figure 3*a***). The far field of the flow induced by a localized force acting perpendicular to a plane no-slip boundary is of the form

$$S_{i3} \sim \frac{1}{4\pi}\left[-\frac{(6+3\delta_{i3})r_i r_3}{r^5} + \frac{15 r_i r_3^3}{r^7}\right], \qquad 8.$$

which decays as $1/r^3$ as r tends to infinity (Blake 1971). Consequently, the component of the cilium motion normal to the cell surface decays rapidly and has no far-field effect. An additional valuable result is that the volume flow rate induced by a parallel-oriented point force is of the form

$$q_{11} := \int_{x_3=0}^{\infty}\int_{x_2=-\infty}^{\infty} S_{11}(\mathbf{x},\mathbf{y})\,\mathrm{d}x_2\,\mathrm{d}x_3 = \frac{y_3}{\pi\mu}, \qquad 9.$$

as given by Liron (1978). Taking integrals out to infinity may appear unrealistic to readers outside the applied mathematics/theoretical physics community! The intended interpretation is as an approximation to the long-range effect of a point force acting near a plane boundary.

A similar image system exists for a rotlet in the presence of a plane boundary, as calculated by Blake & Chwang (1974). The effect of the boundary is perhaps even more dramatic: A rotlet oriented parallel to a plane (representing the tilt component of a rotating cilium) has a far field of the form

$$R_{i\alpha} \sim \frac{3\epsilon_{j\alpha 3} r_i r_j r_3}{4\pi r^5}, \qquad 10.$$

which has a similar form, and hence similar streamlines, to the stresslet far field (Equation 7). Hence, a plane boundary converts a rotational actuation into directional transport, providing a fluid dynamical explanation for the propulsive effect of nodal cilia (Smith et al. 2007). The change from rotational near-field motion to directional far-field motion was confirmed experimentally in a study by Supatto et al. (2008) that tracked fluorescently labeled membrane fragments released by laser ablation (**Figure 3*b***).

The viscous fluid mechanics of boundary interaction were discussed by Brokaw (2005), who observed that, "When tilted posteriorly, movement of the ciliary tip from left to right occurs closer to the cell surface, and surface drag on the fluid limits the ability of the cilium to induce fluid flow from left to right. . . . When the ciliary tip is moving from right to left, it is at its farthest from the surface, and is maximally effective in producing a leftward flow" (p. 43). Okada et al. (2005) also discussed that "Hydrodynamics show that a stationary surface retards the movement of nearby fluid. This makes it difficult for a cilium to move fluid when it is close to a surface. . . . [This may] reduce the angular velocity during the recovery stroke" (p. 636). Combining this explanation with the stresslet nature of the far field yields the picture shown schematically in **Figure 3*c***: Leftward motions achieve a greater effect than rightward motions, thereby resulting in an overall leftward transport of particles.

In a collaborative paper with the same group, Buceta et al. (2005) utilized ideas from polymer dynamics and differential cilium velocity for the leftward and rightward portions of the cilia stroke in order to construct a computational simulation of the flow. However, this explanation does not take full account of the physics of inertialess fluid dynamics: Reduced cilium velocity is a consequence of the presence of the wall but does not cause a reduced propulsive effect due to the time independence of Stokes flow (Smith et al. 2008). The study of Buceta et al. (2005) should, however, be recognized as the first detailed and time-resolved multicilia model of the node. In the next section, we describe techniques for accurate and efficient modeling of multiple cilia, taking into account the nodal geometry.

2.3. Animal Models of Left–Right Symmetry Breaking

In this section, we briefly review the typical animal models of left–right symmetry breaking, outlining some of the dynamically important aspects. More details can be found in the excellent review by Freund et al. (2012). The most commonly studied animal model is the mouse; in addition to the wild type, mutants that have been studied include those deficient in the proteins KIF3B and KIF3A (Nonaka et al. 1998, Takeda et al. 1999), which fail to assemble cilia; the classical *iv*/*iv* immotile cilia mutants, 50% of which have situs inversus; and the more enigmatic inversion of embryonic turning mutants, with faster rotating cilia, slower leftward transport, and 90% situs inversus—in other words, a systematic bias to reversed development. The geometry in the mouse node is relatively easy to visualize: Cilia project from a single near-planar surface with a relatively consistent tilt and rotational direction, and particle transport is to the left around the cilia and to

the right in the upper layer, which is bounded above by Reichert's membrane (further details are given in Section 3).

The equivalent structure in rabbit is the notochordal plate, which is much more elongated than the mouse node and is convex rather than concave. However, the structure still exhibits a similar layer of consistent leftward particle transport, but with the return flow being predominantly at the posterior end of the notochordal plate rather than in an upper deck (Okada et al. 2005). The relevant organ in medakafish, KV, has been shown to take the form of a circular cavity with a convex ciliated floor; the flow has very similar features to the rabbit notochord (Okada et al. 2005). Another genus in which the nodal flow has been studied to some degree is *Xenopus* (Schweickert et al. 2010); by contrast, Hensen's node in the chick embryo appears to break left–right symmetry through a completely different mechanism involving cell migration (Gros et al. 2009).

Symmetry-breaking flow in zebrafish KV has been intensively studied by a number of groups internationally. KV is a fluid-filled cavity that appears transiently at around 12 h postfertilization in the tail region of the embryo, pressed against the yolk sac (**Figure 4**). Motile cilia in KV drive a fluid flow, and as in the mouse, disruption of this activity through interfering with motor proteins (Essner et al. 2005) or intraflagellar transport (Kramer-Zucker et al. 2005) results in situs abnormalities. However, the geometry and actuation of the flow are very different from the mouse node: Cilia project from both the dorsal roof and ventral floor, with clustering toward the anterior end of the dorsal roof (Kreiling et al. 2007, Wang et al. 2012); the dominant flow is anticlockwise (viewed from the dorsal side) rather than leftward (Okabe et al. 2008, Supatto et al. 2008). The tilt direction is also less straightforward, with reports of both dorsal (Supatto et al. 2008) and predominantly posterior (Okabe et al. 2008) tilt [a recent study has reported that cilia are meridionally tilted, which results in dorsal orientation at the equator and posterior orientation at the anterior dorsal roof (Ferreira et al. 2017)]. Cilia in KV typically beat faster than mouse [above 30 Hz in KV compared to about 10 Hz in mouse (Sampaio et al. 2014)] but are fewer in number [50–60 in KV compared to 200–300 in mouse (Freund et al. 2012)]. The KV symmetry-breaking

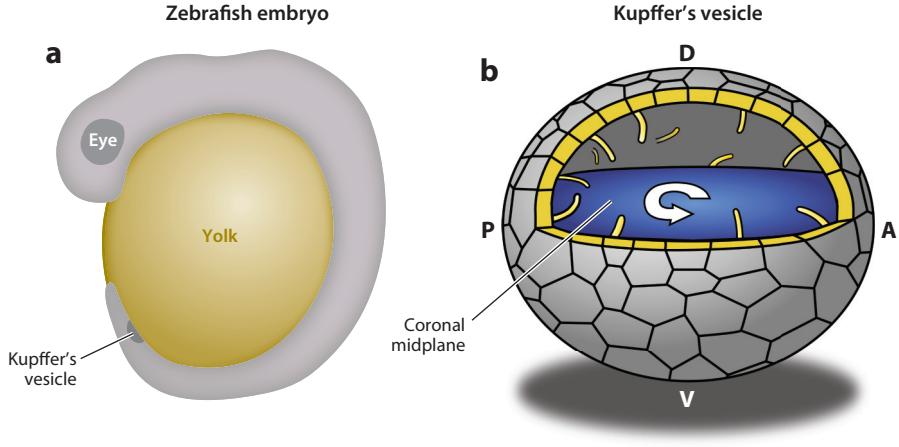

Figure 4

Schematic drawing of Kupffer's vesicle (KV) of zebrafish. (*a*) The zebrafish embryo at approximately 10 h postfertilization, showing KV squeezed between the tail and the yolk sac. (*b*) Cilia protrude into the cavity of KV, creating vortical particle transport in the coronal midplane (midway between dorsal and anterior sides). Panel *b* adapted from Montenegro-Johnson et al. (2016) under CC-BY license 4.0, redrawn from Kreiling et al. (2007). Abbreviations: A, anterior; D, dorsal; P, posterior; V, ventral.

system is remarkably less robust than the mouse, as we discuss in more detail in Section 4. Intuition is inadequate to explore a system of this complexity, so it is essential to formulate mathematical models to augment experiment; some powerful tools to this end are discussed in the next section.

3. MATHEMATICAL MODELING OF NODAL FLOW

We now turn to models that attempt to take into account more of the geometric complexity of the beat cycle, the shape of the node, and the time-dependence of nodal flow. The starting point will be methods based on approximating the slender cilia by line distributions of fundamental solutions to the Stokes flow equations; to progress to whole-organ modeling, we then discuss boundary element and other computational methods.

3.1. Slender Body Models of Cilia

Motivated by the need to retain physical accuracy, along with the ability to predict time-resolved flows and particle trajectories that are accurate in both near and far field, Smith et al. (2007) developed a time-resolved computational model based on line distributions of blakelets combined with the slender body collocation method. The flow field was represented by a line distribution of blakelets for each cilium, combined with higher-order singularities to account for the finite radius of the cilium. Denoting the resulting singular kernel by G_{ij}, the flow field due to N cilia with centerline shape $\mathbf{X}^{(n)}(s,t)$ for $n = 1, \ldots, N$ can then be expressed as

$$u_i(\mathbf{x},t) = \sum_{n=1}^{N} \int_0^L G_{ij}[\mathbf{x}, \mathbf{X}^{(n)}(s,t)]\, f_j^{(n)}(s,t)\, \mathrm{d}s. \qquad 11.$$

Taking a piecewise constant discretization of the force per unit length $\mathbf{f}^{(n)}(s,t)$ and imposing the no-slip, no-penetration condition, $\mathbf{u}(\mathbf{X}^{(n)},t) = \dot{\mathbf{X}}^{(n)}$, on one surface point per segment per cilium yields a (dense) linear system that can be solved for the force distribution. The flow field, and hence particle paths, can then be calculated.

Smith et al. (2007) modeled only one to three cilia; however, certain properties of cilia-driven transport were revealed. First, Lagrangian particles undergo large oscillations during the beat cycle, with large forward movement during the leftward stroke, followed by small backward movement during the rightward stroke. (However, these findings should be interpreted with Brownian motion in mind: Submicron particles will also undergo significant displacements during the time taken for a single beat cycle.) Second, particles may be transported from the vicinity of one cilium to another, become trapped in an orbit around the leftward cilium, and escape following an extended period of orbit. Third, cilia synchronization is unnecessary to affect transport; however, changes to relative phase may significantly alter particle trajectories. Fourth, there is no rightward flow layer close to the cell surface; particles released at or below the cilium tips were never observed migrating rightward. The slender body collocation method is very computationally inexpensive when compared with finite element methods because the unknowns are reduced to a small number of 1D line segments; these results were hence extended to larger arrays (Smith et al. 2008).

An additional important bounding surface in the node is the upper Reichert's membrane, which produces a closed cavity. Experiments with cultured embryos, such as those of Nonaka et al. (1998), necessarily removed this membrane, and the mathematical model of Smith et al. (2007) took the lower surface into account but represented the fluid as being unbounded in the positive x_3 direction. Cartwright et al. (2007) posed the question of how the upper membrane

present in vivo would alter the flow dynamics through a 3D (although time-averaged) computer model based on a finite element discretization of the Navier–Stokes equations. They predicted a counterflow to the right occurring in an upper layer, counterbalancing the leftward transport just above the cilia tips. We return to the issue of the overlying membrane shortly.

The study of Smith et al. (2008) could perhaps be characterized as a mathematical model inspired by an experimental model of an animal model! The experimental model was that of Nonaka et al. (2005) described above: a rotating wire in a viscous fluid. A straight wire undergoing tilted conical rotations can be described by the formula $\mathbf{X}(s,t) = s\,\mathbf{T}(t)$, where s is arclength, t is time, and the tangent vector is

$$\mathbf{T}(t) = \begin{pmatrix} \sin\psi\cos(\omega t) \\ -\sin\psi\sin(\omega t)\cos\theta - \cos\psi\sin\theta \\ -\sin\psi\sin(\omega t)\sin\theta + \cos\psi\cos\theta \end{pmatrix}. \tag{12.}$$

This parameterization represents motion through a conical envelope with semicone angle ψ, tilt toward the negative x_2 (posterior) axis by angle θ, and clockwise rotation (viewed from tip to base) with angular velocity ω. The velocity of this rotation is normal to the cilium axis, enabling the force per unit length exerted by the cilium on the fluid to be expressed via the resistive force theory of Gray & Hancock (1955),

$$\mathbf{f} \approx C_{\mathrm{T}}(\dot{\mathbf{X}}\cdot\mathbf{T})\mathbf{T} + C_{\mathrm{N}}[(\dot{\mathbf{X}}\cdot\mathbf{N})\mathbf{N} + (\dot{\mathbf{X}}\cdot\mathbf{B})\mathbf{B}], \tag{13.}$$

$$= C_{\mathrm{N}}\dot{\mathbf{X}}, \tag{14.}$$

where $\{\mathbf{T},\mathbf{N},\mathbf{B}\}$ form an orthogonal basis, with $\dot{\mathbf{X}}\cdot\mathbf{T} = 0$, and C_{N} and C_{T} are normal and tangential resistance coefficients, respectively. The main effect of the boundary on the flow was taken into account via the use of the blakelet image system given in Equation 5. Hence, the instantaneous fluid velocity due to a straight, rotating cilium of length L could be expressed via the line integral

$$u_i(\mathbf{x},t) = \int_0^L B_{ij}[\mathbf{x},\mathbf{X}(s,t)]\,f_j(s,t)\,\mathrm{d}s, \tag{15.}$$

$$\approx \int_0^L B_{ij}[\mathbf{x},\mathbf{X}(s,t)]C_{\mathrm{N}}\dot{X}_j\,\mathrm{d}s, \tag{16.}$$

and the time-averaged volume flow rate in the x_1 (positive leftward) direction could be expressed by

$$Q = \frac{\omega}{2\pi}\int_{t=0}^{2\pi/\omega}\int_{x_3=0}^{\infty}\int_{x_2=-\infty}^{\infty} u_1(\mathbf{x},t)\,\mathrm{d}x_2\,\mathrm{d}x_3\,\mathrm{d}t. \tag{17.}$$

Noting the formula for volume flow rate (Equation 9), using the resistive force theory of Equation 16, and evaluating time integrals of trigonometric functions, we get a compact expression for the time-averaged volume flow rate in terms of the geometric parameters ψ and θ:

$$Q \approx \frac{C_{\mathrm{N}}\omega L^3}{6\pi\mu}\sin^2\psi\sin\theta. \tag{18.}$$

This expression immediately yields that the optimum volume flow rate is achieved when $\psi = \arctan\sqrt{2} \approx 54.7°$ and $\theta = 35.3°$ ($\psi + \theta = 90°$) and, moreover, that values of $\psi = 60°$ and $\theta = 30°$ yield slightly more transport than $\psi = 45° = \theta$, as observed by Nonaka et al. (2005). Biological measurements of tilt angle of immotile cilia in the *iv/iv* mouse node yielded an estimate of $\theta = 27°$ (although within-embryo averages were 15–35°) (Nonaka et al. 2005), while analysis of videomicroscopy data of motile cilia showed ranges of approximately 25–55° in mouse, 25–45° in rabbit,

and 27–55° in medakafish (reanalysis of data was presented in Okada et al. 2005). Vilfan (2012) further generalized the simplified model to yield the full spatial dependence of the time-averaged flow due to a tilted rotating cilium—in addition to other models of propulsion. We return to this formula in Section 4.2 when we discuss the effect of perturbations to cilium length. Montenegro-Johnson et al. (2016) used a similar approach to calculate the moment generated by the time-averaged rotational motion in order to construct a whole-organ time-averaged flow model of zebrafish KV.

3.2. Boundary Element Methods of the Organizing Structure

Returning to the issue of modeling the overlying Reichert's membrane, Smith et al. (2011) made use of a hybrid slender body/regularized Stokeslet boundary element method as a way to retain time resolution without incurring excessive additional computational cost. The regularized Stokeslet (Cortez 2001, Cortez et al. 2005) is the solution to the Stokes flow equations with spatially smoothed force per unit volume $\phi_\epsilon(\mathbf{x}-\mathbf{y})$:

$$-\nabla p + \nabla^2 \mathbf{u} + 8\pi \mathbf{e}_k \phi_\epsilon(\mathbf{x}-\mathbf{y}) = 0, \quad \nabla \cdot \mathbf{u} = 0. \tag{19.}$$

A frequently used form for 3D flow is based on the smoothed point force,

$$\phi_\epsilon(\xi) = \frac{15\epsilon^4}{8\pi(|\xi|^2+\epsilon^2)^{7/2}}, \tag{20.}$$

where $0 < \epsilon \ll 1$ is a regularization parameter. This choice leads to the regularized Stokeslet velocity tensor:

$$S^\epsilon_{ij}(\mathbf{x},\mathbf{y}) = \delta_{ij}\frac{|\mathbf{x}-\mathbf{y}|^2+\epsilon^2}{(|\mathbf{x}-\mathbf{y}|^2+\epsilon^2)^{3/2}} + \frac{(x_i-y_i)(x_j-y_j)}{(|\mathbf{x}-\mathbf{y}|^2+\epsilon^2)^{3/2}}. \tag{21.}$$

The original nonregularized formulation of the boundary element method based on the singular Stokeslet is well established (Pozrikidis 1992); an advantage of the regularized version, however, is that the fluid velocity field is numerically straightforward to evaluate even in the vicinity of cilia and flagella.

Ainley et al. (2008) derived a regularized version of the blakelet for this point force, which we denote by B^ϵ_{ij}. Stokes flow driven by N rotating cilia projecting from the no-slip, no-penetration surface, $x_3 = 0$, below an impermeable boundary M (depicted with a wire frame in **Figure 5*a***) can be expressed via the hybrid slender body/regularized Stokeslet boundary integral equation:

$$u_i(\mathbf{x},t) = \sum_{n=1}^{N}\int_0^L B^\epsilon_{ij}[\mathbf{x},\mathbf{X}_n(s,t)]f_j^{(n)}(s,t)\,\mathrm{d}s + \iint_M B^\epsilon_{ij}(\mathbf{x},\mathbf{y})\Phi_j(\mathbf{y},t)\,\mathrm{d}S_\mathbf{y}. \tag{22.}$$

Equation 22 can again be efficiently solved for the force per unit length $f_j^{(n)}(s,t)$ and stress $\Phi_j(\mathbf{y})$ via a constant element discretization and collocation (Smith et al. 2011); flow fields and particle paths can then be calculated, enabling the identification of the average leftward and rightward flow regions (identified in **Figure 5*b***). The use of an element-type discretization significantly improves accuracy and efficiency over the standard method of regularized Stokeslets (Smith 2009). Time-resolved particle tracking showed that in the presence of an overlying membrane, the membrane halts particle migration beyond the left-hand edge of the cilia array: Once a particle has moved to the left of the cilia, it lifts up and joins the upper deck return flow region. Particles do not continue ballistically toward the edge of the node (**Figure 6**). Further modeling of the gradual increase in cilia number and posterior tilt angle associated with the stages of embryo development (Hashimoto et al. 2010) elucidated qualitative changes in particle trajectories (Montenegro-Johnson et al. 2012). A limitation of the above studies involving Lagrangian particle tracking is that any particles of biochemical influence are likely to be submicron in size, and hence, Brownian effects are important.

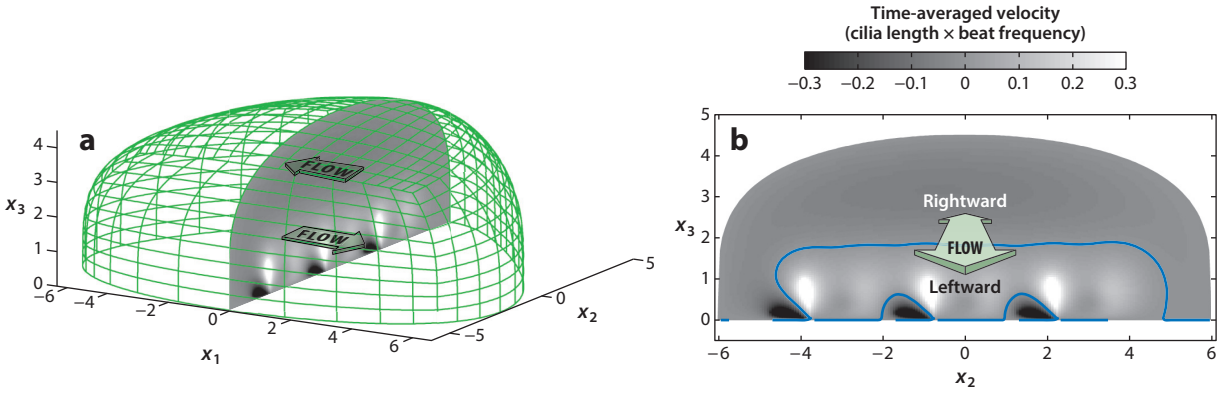

Figure 5

Hybrid slender body/regularized Stokeslet boundary integral modeling of flow generation by an array of tilted cilia, taking into account the hydrodynamic effect of the nodal floor via the regularized blakelet and the upper membrane via a surface integral of regularized Stokeslets. (*a*) Isometric view of the geometry of the model of the overlying Reichert's membrane of Smith et al. (2011). The density plot depicts the time-averaged leftward flow (positive is leftward and negative is rightward). (*b*) Sagittal cross section (the anterior/posterior–dorsal/ventral plane) with thin blue lines demarking time-averaged leftward and rightward flows. Figure adapted with permission from Smith et al. (2011), copyright 2010 Springer.

To model the more complex system of KV, Smith et al. (2012) constructed a moving mesh $M(t)$ of the bounding surface and cilia. Using a Voronoi tesselation with varying cell size enabled the simulation of varying cilia densities, as reported by Kreiling et al. (2007). The mathematical model then takes the form

$$u_j(\mathbf{x}, t) = \iint_{M(t)} S^{\epsilon}_{jk}(\mathbf{x}, \mathbf{y}) \Phi_k(\mathbf{y}) \, \mathrm{d}S_{\mathbf{y}}, \qquad 23.$$

where $\mathbf{\Phi}(\mathbf{y})$ is the surface stress. This equation is then solved similarly to the models above by collocation, taking $\mathbf{u}(\mathbf{X}, t) = \dot{\mathbf{X}}$ for all $\mathbf{X} \in M(t)$. An example computational mesh with a calculated time-averaged flow field is depicted in **Figure 7*a***, alongside particle tracking results (**Figure 7*b***).

Smith et al. (2012) found that a combination of posterior tilt on the roof and floor and dorsal tilt around the equator produces flow closest to that observed by Okabe et al. (2008). A conceptual model (Smith et al. 2014) of this tilt distribution is shown in **Figure 7*c–e***. The posterior-tilted dorsal roof and ventral floor produce transport in opposite directions. However, the dorsal–anterior cluster dominates the other regions; the dorsal-tilted equatorial cilia produce an additional anticlockwise circulating component. These modeling techniques were then applied to interpret results from experiments with perturbed cilia length and number, as described in Section 4.

Other modeling techniques that should be mentioned include the use of finite element analysis (Chen & Zhong 2015) to explain the emergence of cilia rotation from internal axoneme structure and hybrid boundary element/finite element multiscale modeling, which couples suborganelle structural detail to external flow dynamics (Omori et al. 2017); as computational techniques and technology develop further, models of this type are likely to become more widespread and will be particularly valuable in probing mechanical sensing of flow.

4. PERTURBING THE NODAL FLOW

A typical feature of biological studies of the left–right organizer has been the use of mutants and genetic manipulation to push the system to a breaking point (or perhaps nonbreaking point) in terms of cilia numbers, length, or motility.

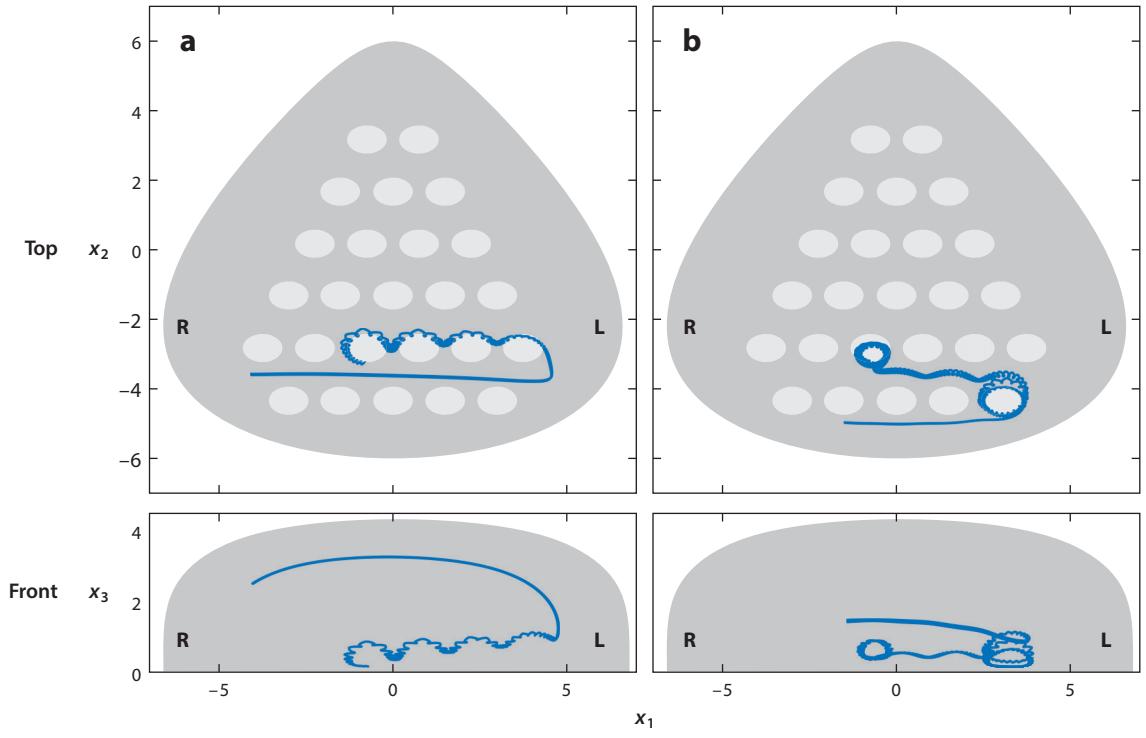

Figure 6

Lagrangian particle tracks from time-resolved hybrid slender body/regularized Stokeslet boundary element computation, taking account of the hydrodynamic effect of the nodal floor and overlying Reichert's membrane. Note the convention that the right (R) and left (L) of the embryo are depicted on the left-hand and right-hand sides of the figure, respectively. The red arrows indicate the initial position of the particle. In panel *a*, the initial position (x_1, x_2, x_3) is at $(-0.75L, -3.25L, 0.1L)$, where L is cilium length. In panel *b*, the initial position is as in panel *a* but with $x_3 = 0.3L$. Particle paths are strongly affected by the nearest cilium/cilia and may become transiently trapped in several orbits. Fine-scale looping behavior is the result of the highly oscillatory flow field. The presence of the overlying membrane causes particles to lift above the cilium array and return to the right. A small perturbation to initial position can result in a dramatically altered particle path. Figure adapted with permission from Smith et al. (2011), copyright 2010 Springer.

4.1. Cilia Numbers

The most dramatic example of this approach was the study of Shinohara et al. (2012). Embryos with nodal flow drastically attenuated by raised viscosity (**Figure 8**) produced almost normal gene expression asymmetry; still more surprisingly, *Dpcd*- and *Rfx3*-mutant embryos with just two motile cilia showed nearly perfectly consistent normal symmetry breaking, again despite drastically reduced flow. These findings were interpreted as suggesting a mechanosensing mechanism over NVP transport, with the caveat that a system must exist for broadcasting a signal from a small number of leftward sensory cells.

The system in KV is much less robust. Even in wild-type fish, only around 90% of embryos achieve normal situs, so cilia have the effect of biasing a random system rather than robustly ensuring normal development. In the *deltaD*$^{-/-}$ (*dld*$^{-/-}$) mutant, reductions in motile cilia number and cilia length (from about a mean value of 4 to 3.5 μm) reduce the strength of this forcing and hence weaken the biasing mechanism so that only 60% of embryos develop normally (Sampaio et al. 2014, Smith et al. 2014). Strong anterior flow and strong flow on the left of the embryo are both associated with normal situs; simulations of many randomly generated virtual KV suggest

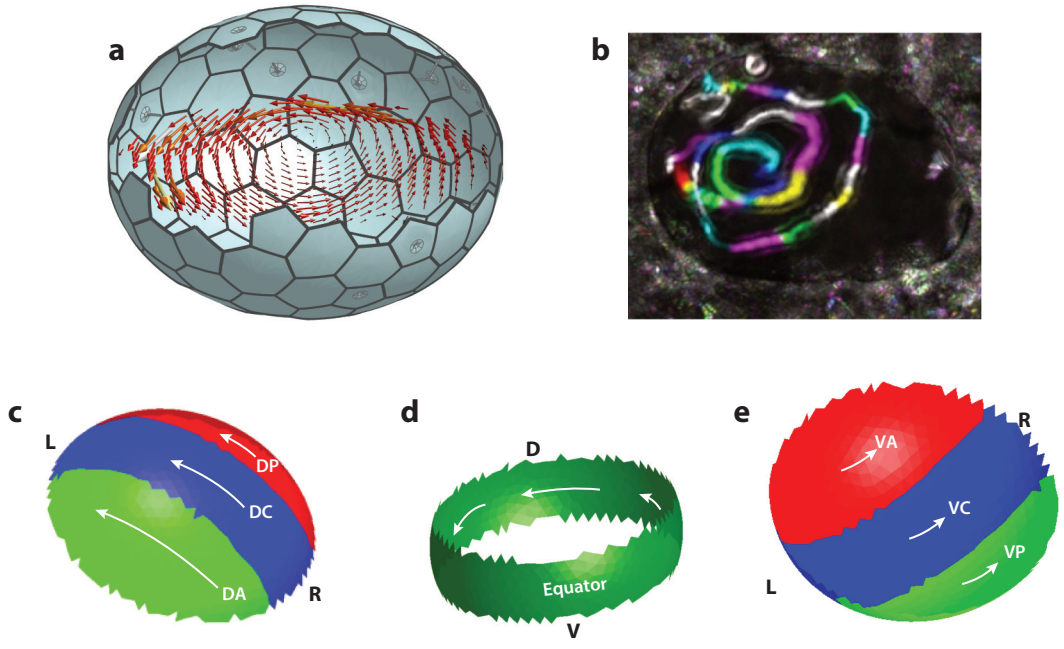

Figure 7

Computational modeling, experimental observations, and a conceptual model of transport in Kupffer's vesicle (KV) of zebrafish. (*a*) Time-averaged fluid flow produced by a randomly generated computational model of KV with 32 cilia. (*b*) Particle tracking results, emphasizing the rotational component of the flow. Panels *a* and *b* adapted with permission from Sampaio et al. (2014), copyright 2014 Elsevier. (*c–e*) Conceptual model of transport in KV with posterior tilt on the dorsal roof and ventral floor and dorsal tilt around the equator; transport can be deconstructed as the sum of components from each section, with the dorsal-anterior clustering having the strongest effect. Panels *c–e* adapted with permission from Smith et al. (2014). Abbreviations: A, anterior; C, center; D, dorsal; L, left; P, posterior; R, right; V, ventral.

that to achieve the flow features associated with situs solitus, around 30 motile cilia are required (Sampaio et al. 2014). While strong anterior flow may be expected as an indicator of anterior clustering of motile cilia, strong flow on the left side is less straightforward to interpret, as the cilia placement is expected to be initially statistically uniform in the left–right axis. Is an increase in cilia expression or motility on the left an early, self-reinforcing event?

4.2. Cilia Length, Beat Pattern, and Organ Size

The L^3 dependence of Equation 18 was effective in explaining, along with reduced numbers, the dramatic reduction in flow velocity observed in *dld*$^{-/-}$-mutant embryos with short cilia. However, in vesicles engineered to grow longer cilia through an injection of *arl13b* messenger RNA (Pintado et al. 2017), Equation 18 breaks down due to a change in the cilia beat pattern. The rigidity of a beating cilium is determined by the relative importance of viscous to elastic forces, which can be quantified via the dimensionless group $\chi = \omega\mu L^4/E$, where E is bending rigidity (Qian et al. 2008). A change in the average length from 6.4 μm (wild type) to 9.5 μm (injected) moves χ through the straight-to-helical transition range. Above the helical transition length, the cilia beat amplitude assumes a smaller, length-independent value, which we denote a. Dimensional analysis then yields that the moment exerted by a whirling cilium—and hence the flow produced—scales with $a^2 L$ (the formula of Equation 18 can be reinterpreted in this way with $a = L \sin \psi$). This finding suggests

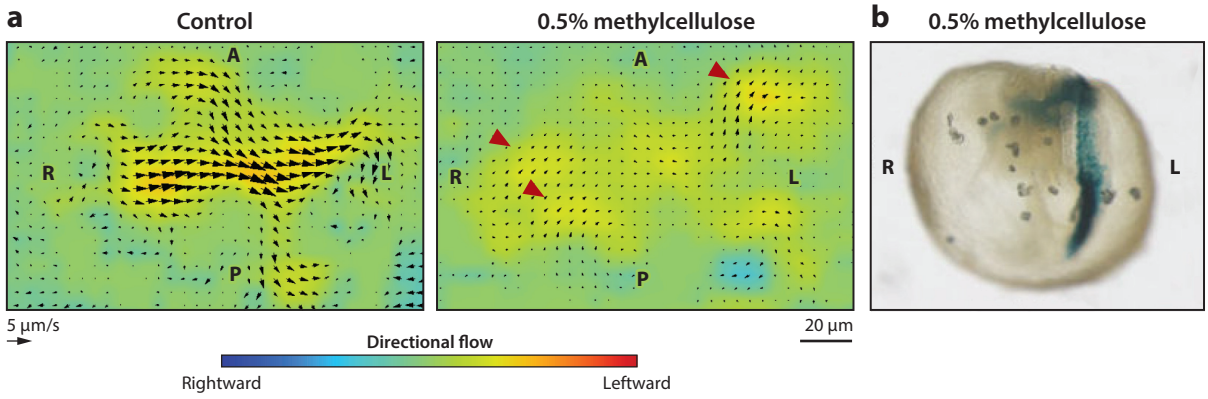

Figure 8

Particle image velocimetry and asymmetric gene expression data from mouse embryos. (*a*) Control embryo (*left*) versus an embryo with a culture medium supplemented with 0.5% methylcellulose (*right*) to raise viscosity and hence reduce cilia beat frequency and fluid velocity; red arrows denote local leftward directional flow. Time-averaged fluid velocity distributions were calculated over an interval of 10 s. (*b*) Asymmetric expression of *Pitx2* visualized via a reporter transgene from an embryo cultured in 0.5% methylcellulose. Figure adapted with permission from Shinohara et al. (2012), copyright 2012 Springer Nature. Abbreviations: A, anterior; L, left; P, posterior; R, right.

that wild-type cilia length is optimal in producing transport (Pintado et al. 2017). Longer cilia have also been induced via *S6k1* overexpression (Yuan et al. 2012); this system additionally results in a significant reduction in cilia beat frequency ω and hence a strong reduction of fluid velocity.

KV size, measured by lumen area, has also been shown to be a factor in biasing development toward normal symmetry breaking. A study of a range of zebrafish variants revealed that a KV lumen area of $\leq$1,300 μm^2 is associated with reduced flow and a loss of asymmetric gene expression, despite cilia numbers not being significantly altered (Gokey et al. 2016). The precise mechanism for this effect is unclear; potential explanations may involve changes to cilia motility, tilt direction, or morphogen concentration.

5. FUTURE DIRECTIONS

5.1. Mechanisms of Flow Conversion

Flow conversion is undoubtedly the central question of nodal cilia research. Since the 2009 review by Hirokawa and colleagues, Yoshiba et al. (2012) discovered that the cation channel Pkd2 in the ciliary crown cells is essential for symmetry breaking and that restoring cilia in the crown cells of KIF3A mutants restored flow response. Yuan et al. (2015) showed that asymmetric calcium oscillations coincide with the appearance of motile cilia. The data of Shinohara et al. (2012) discussed above were also interpreted as supporting a mechanosensing over a chemosensing mechanism. Our group (Sampaio et al. 2014, Montenegro-Johnson et al. 2016) also interpreted the importance of strong flow at the anterior and left as being consistent with a mechanosensing process. However, Delling et al. (2016) reported that cilia are not capable of sensing force via a calcium signal (see Norris & Jackson 2016 for further discussion), creating a paradox that is yet to be resolved. Ferreira et al. (2017) have argued through mathematical modeling that the number of motile cilia in KV is too small for directional mechanosensing because the flow is below the detection threshold for cilia-based mechanosensing. They explored the possibility that cilia may detect their own position from the differential torques generated during anterior and posterior motions;

however, it was argued that the most probable model was based on asymmetric vesicle secretion in the anterior followed by transport to the left.

Returning to the landmark paper of Okada et al. (2005), it was observed that the rightward sweep of the cilium just above the cell surface might facilitate the release of morphogen bound to the lipid membrane or extracellular matrix—in other words, a hybrid process involving both mechanical stimulation and morphogen transport. Uncovering the full process likely requires this type of integrative thinking: The truth may not be "mechanics or morphogens" but rather "mechanics and morphogens." It may of course also be that mammals and fish have diverged sufficiently that the process in one is unlike that in the other—in the same way that avian symmetry breaking does not appear to involve flow at all.

5.2. Does a Unidirectional Nodal Flow Exist?

This question may seem provocative! After all, there is a wealth of observational evidence, supported by mathematical and computational analyses, that definitively shows consistent and statistically significant particle transport to the left of the embryo and the underpinning fluid mechanics of unidirectional nodal flow. Moreover, flow reversal has been known for some time to restore situs in mutant embryos (Nonaka et al. 2002). However, the key issue here is that we are only able to measure particle transport, and only then with a finite time resolution. This issue of time resolution cannot be solved simply by using a higher–frame rate camera—it is intrinsic to the use of Brownian particles to measure flow. The PIV flow plot data of Shinohara et al. (2012) correspond to the order of one hundred beat cycles; long-time particle tracking data (Sampaio et al. 2014) reveal the statistical average of the flow but not the fine-timescale oscillatory nature. Time-resolved mathematical modeling (Smith et al. 2007, 2008, 2011) emphasizes that particles encounter a flow field that rapidly alternates between moving left and right, with a leftward bias that produces flow. Moreover, the flow produced by an individual cilium is quite localized (on the order of $1/r^2$); the motion of the fluid close to a cilium is predominantly determined by that particular cilium. When formulating conceptual models of the system, it is therefore essential to take into account the fact that the fluid flow is oscillatory with leftward bias and spatially uneven, being much stronger in the vicinity of a cilium. In this respect, we can be more precise by saying that there is a nodal drift of particles to the left, which is produced by a biased, oscillating, and spatially uneven flow field.

Another aspect that has previously been discussed extensively but is still worth repeating is that we must always keep in mind the counterintuitive nature of inertialess flow. In particular, cilia do not produce a leftward-directed jet in the manner of a set of propellers; rather, the flow each cilium produces is symmetric with respect to decay and the shape of streamlines (**Figure 3**). Moreover, fluid momentum produced by cilia does not travel; rather, the flow is instantaneously determined by the cilia movement. This intuition is crucial when interpreting the mechanosensing hypothesis: The conceptual model of **Figure 2*c*** could be made more accurate by adding a flow arrow upstream of the cilia. Moreover, the flow at the periphery on the left and right is weaker than the flow in the center. Conversely, mathematical modelers should always be aware of the noisy nature of the system under consideration—the inclusion of Brownian effects in particle tracking simulation is an important example of this for future work.

6. CONCLUSION

Uncovering the process of left–right symmetry breaking takes us from a familiar, macroscale anatomical fact down to an intricate fluid mechanical process taking place in a miniscule, delicate

structure in early development. After decades of speculation, rapid progress was made in uncovering the key features of how the flow is generated. The last ten years of interdisciplinary research have produced surprises, some illumination, and many more questions. The process of left–right organization is an exemplar of the complexity of biology and the need for an interdisciplinary approach, as it involves genetics, advection-diffusion-reaction and/or electrophysiology, continuum mechanics, geometry, and probability. Key questions for the future include (*a*) definitively resolving which conversion processes are compatible with the known data in both fish and mammals. The recent study of Ferreira et al. (2017) is an excellent example of the type of integrative reasoning required. (*b*) It must be resolved whether mechanosensing via calcium signaling is possible—this will involve a technical investigation of experimental techniques and associated artifacts. (*c*) The multiscale nature of the system must be taken into account, in both timescales (the beat period of 0.1 s to hours or days of development) and spatial scales (from nanometer-scale intraciliary structures and morphogen-containing vesicles to tens of microns across the organizing structure). (*d*) Mechanical and organ growth/remodeling effects must also be integrated. (*e*) The randomness associated with biological processes involving tens of cells or cilia must be incorporated. (*f*) The correct physics must be brought to bear on the problem, including both viscous flow dynamics and Brownian effects, as appropriate.

DISCLOSURE STATEMENT

The authors are not aware of any biases that might be perceived as affecting the objectivity of this review.

ACKNOWLEDGMENTS

D.J.S. acknowledges funding from an Engineering and Physical Sciences Research Council (EPSRC) Healthcare Technologies Challenge Award (EP/N021096/1); D.J.S. and T.D.M.-J. acknowledge funding from EPSRC First Grant EP/K007637/1. T.D.M.-J. acknowledges a Royal Commission for the Exhibition of 1851 Research Fellowship. S.S.L. acknowledges funding from Fundação para a Ciência e a Tecnologia (FCT-ANR/BEX-BID/0153/2012 research grant) and FCT Investigator award IF/00951/2012.

We are particularly grateful for the guidance and encouragement of Professor Julyan Cartwright and the late Professor John Blake. We thank colleagues Dr. Adán Guerrero and Dr. Idan Tuval and current and former members of the Lisbon and Birmingham groups for their valuable contributions.

LITERATURE CITED

Afzelius B. 1976. A human syndrome caused by immotile cilia. *Science* 193:317–19

Ainley J, Durkin S, Embid R, Boindala P, Cortez R. 2008. The method of images for regularized Stokeslets. *J. Comput. Phys.* 227:4600–16

Berdon W, McManus C, Afzelius B. 2004. More on Kartagener's syndrome and the contributions of Afzelius and A.K. Siewert. *Pediatr. Radiol.* 34:585–86

Berdon W, Willi U. 2004. Situs inversus, bronchiectasis, and sinusitis and its relation to immotile cilia: history of the diseases and their discoverers—Manes Kartagener and Bjorn Afzelius. *Pediatr. Radiol.* 34:38–42

Blake J. 1971. A note on the image system for a stokeslet in a no-slip boundary. *Math. Proc. Camb. Philos. Soc.* 70:303–10

Blake J, Chwang A. 1974. Fundamental singularities of viscous flow. *J. Eng. Math.* 8:23–29

Blum M, Feistel K, Thumberger T, Schweickert A. 2014. The evolution and conservation of left-right patterning mechanisms. *Development* 141:1603–13
Brokaw C. 2005. Computer simulation of flagellar movement IX. Oscillation and symmetry breaking in a model for short flagella and nodal cilia. *Cell Motil. Cytoskel.* 60:35–47
Brueckner M. 2001. Cilia propel the embryo in the right direction. *Am. J. Med. Genet. A* 101:339–44
Buceta J, Ibañes M, Rasskin-Gutman D, Okada Y, Hirokawa N, Izpisúa-Belmonte J. 2005. Nodal cilia dynamics and the specification of the left/right axis in early vertebrate embryo development. *Biophys. J.* 89:2199–209
Cartwright J, Piro N, Piro O, Tuval I. 2007. Embryonic nodal flow and the dynamics of nodal vesicular parcels. *J. R. Soc. Interface* 4:49–56
Cartwright J, Piro O, Tuval I. 2004. Fluid-dynamical basis of the embryonic development of left-right asymmetry in vertebrates. *PNAS* 101:7234–39
Chen D, Zhong Y. 2015. A computational model of dynein activation patterns that can explain nodal cilia rotation. *Biophys. J.* 109:35–48
Cortez R. 2001. The method of regularized Stokeslets. *SIAM J. Sci. Comput.* 23:1204–25
Cortez R, Fauci L, Medovikov A. 2005. The method of regularized Stokeslets in three dimensions: analysis, validation, and application to helical swimming. *Phys. Fluids* 17:031504
Delling M, Indzhykulian A, Liu X, Li Y, Xie T, et al. 2016. Primary cilia are not calcium-responsive mechanosensors. *Nature* 531:656–60
Eloy C, Lauga E. 2012. Kinematics of the most efficient cilium. *Phys. Rev. Lett.* 109:038101
Essner J, Amack J, Nyholm M, Harris E, Yost H. 2005. Kupffer's vesicle is a ciliated organ of asymmetry in the zebrafish embryo that initiates left-right development of the brain, heart and gut. *Development* 132:1247–60
Ferreira R, Vilfan A, Jülicher F, Supatto W, Vermot J. 2017. Physical limits of flow sensing in the left-right organizer. *eLife* 6:e25078
Freund J, Goetz J, Hill K, Vermot J. 2012. Fluid flows and forces in development: functions, features and biophysical principles. *Development* 139:1229–45
Gokey J, Ji Y, Tay H, Litts B, Amack J. 2016. Kupffer's vesicle size threshold for robust left–right patterning of the zebrafish embryo. *Dev. Dyn.* 245:22–33
Gray J, Hancock G. 1955. The propulsion of sea-urchin spermatozoa. *J. Exp. Biol.* 32:802–14
Gros J, Feistel K, Viebahn C, Blum M, Tabin C. 2009. Cell movements at Hensen's node establish left/right asymmetric gene expression in the chick. *Science* 324:941–44
Handel M, Kennedy J. 1984. Situs inversus in homozygous mice without immotile cilia. *J. Hered.* 75:498
Hashimoto M, Shinohara K, Wang J, Ikeuchi S, Yoshiba S, et al. 2010. Planar polarization of node cells determines the rotational axis of node cilia. *Nat. Cell Biol.* 12:170–76
Hirokawa N, Okada Y, Tanaka Y. 2009. Fluid dynamic mechanism responsible for breaking the left-right symmetry of the human body: the nodal flow. *Annu. Rev. Fluid Mech.* 41:53–72
Hirokawa N, Tanaka Y, Okada Y, Takeda S. 2006. Nodal flow and the generation of left-right asymmetry. *Cell* 125:33–45
Hummel K, Chapman D. 1959. Visceral inversion and associated anomalies in the mouse. *J. Hered.* 50:9–13
Kramer-Zucker A, Olale F, Haycraft C, Yoder B, Schier A, Drummond I. 2005. Cilia-driven fluid flow in the zebrafish pronephros, brain and Kupffer's vesicle is required for normal organogenesis. *Development* 132:1907–21
Kreiling J, Williams G, Creton R. 2007. Analysis of Kupffer's vesicle in zebrafish embryos using a cave automated virtual environment. *Dev. Dyn.* 236:1963–69
Levin M, Johnson R, Sterna C, Kuehn M, Tabin C. 1995. A molecular pathway determining left-right asymmetry in chick embryogenesis. *Cell* 82:803–14
Liron N. 1978. Fluid transport by cilia between parallel plates. *J. Fluid Mech.* 86:705–26
Lopes S, Lourenço R, Pacheco L, Moreno N, Kreiling J, Saúde L. 2010. Notch signalling regulates left-right asymmetry through ciliary length control. *Development* 137:3625–32
McGrath J, Somlo S, Makova S, Tian X, Brueckner M. 2003. Two populations of node monocilia initiate left-right asymmetry in the mouse. *Cell* 114:61–73
Montenegro-Johnson T, Baker D, Smith D, Lopes S. 2016. Three-dimensional flow in Kupffer's vesicle. *J. Math. Biol.* 73:705–25

Montenegro-Johnson T, Smith A, Smith D, Loghin D, Blake J. 2012. Modelling the fluid mechanics of cilia and flagella in reproduction and development. *Eur. Phys. J. E* 35:1–17
Nonaka S, Shiratori H, Saijoh Y, Hamada H. 2002. Determination of left–right patterning of the mouse embryo by artificial nodal flow. *Nature* 418:96–99
Nonaka S, Tanaka Y, Okada Y, Takeda S, Harada A, et al. 1998. Randomization of left–right asymmetry due to loss of nodal cilia generating leftward flow of extraembryonic fluid in mice lacking KIF3B motor protein. *Cell* 95:829–37
Nonaka S, Yoshiba S, Watanabe D, Ikeuchi S, Goto T, et al. 2005. De novo formation of left–right asymmetry by posterior tilt of nodal cilia. *PLOS Biol.* 3:e268
Norris D. 2012. Cilia, calcium and the basis of left-right asymmetry. *BMC Biol.* 10:102
Norris D, Jackson P. 2016. Cell biology: calcium contradictions in cilia. *Nature* 531:582
Okabe N, Xu B, Burdine R. 2008. Fluid dynamics in zebrafish Kupffer's vesicle. *Dev. Dyn.* 237:3602–12
Okada Y, Nonaka S, Tanaka Y, Saijoh Y, Hamada H, Hirokawa N. 1999. Abnormal nodal flow precedes situs inversus in iv and inv mice. *Mol. Cell* 4:459–68
Okada Y, Takeda S, Tanaka Y, Belmonte JC, Hirokawa N. 2005. Mechanism of nodal flow: a conserved symmetry breaking event in left-right axis determination. *Cell* 121:633–44
Omori T, Sugai H, Imai Y, Ishikawa T. 2017. Nodal cilia-driven flow: development of a computational model of the nodal cilia axoneme. *J. Biomech.* 61:242–49
Pennekamp P, Menchen T, Dworniczak B, Hamada H. 2015. Situs inversus and ciliary abnormalities: 20 years later, what is the connection? *Cilia* 4:1
Pintado P, Sampaio P, Tavares B, Montenegro-Johnson T, Smith D, Lopes S. 2017. Dynamics of cilia length in left–right development. *R. Soc. Open Sci.* 4:161102
Pozrikidis C. 1992. *Boundary Integral and Singularity Methods for Linearized Viscous Flow*. Cambridge, UK: Cambridge Univ. Press
Qian B, Powers T, Breuer K. 2008. Shape transition and propulsive force of an elastic rod rotating in a viscous fluid. *Phys. Rev. Lett.* 100:078101
Sampaio P, Ferreira R, Guerrero A, Pintado P, Tavares B, et al. 2014. Left-right organizer flow dynamics: How much cilia activity reliably yields laterality? *Dev. Cell* 29:716–28
Schoenwolf G, Bleyl S, Brauer P, Francis-West P. 2014. *Larsen's Human Embryology*. Philadelphia: Churchill Livingsone. 5th ed.
Schweickert A, Ott T, Kurz S, Tingler M, Maerker M, et al. 2018. Vertebrate left-right asymmetry: What can nodal cascade gene expression patterns tell us? *J. Cardiovasc. Dev. Dis.* 5:1
Schweickert A, Vick P, Getwan M, Weber T, Schneider I, et al. 2010. The nodal inhibitor *Coco* is a critical target of leftward flow in *Xenopus*. *Curr. Biol.* 20:738–43
Schweickert A, Weber T, Beyer T, Vick P, Bogusch S, et al. 2007. Cilia-driven leftward flow determines laterality in *Xenopus*. *Curr. Biol.* 17:60–66
Shinohara K, Hamada H. 2017. Cilia in left–right symmetry breaking. *Cold Spring Harb. Perspect. Biol.* 9:a028282
Shinohara K, Kawasumi A, Takamatsu A, Yoshiba S, Botilde Y, et al. 2012. Two rotating cilia in the node cavity are sufficient to break left–right symmetry in the mouse embryo. *Nat. Commun.* 3:622
Smith A, Johnson T, Smith D, Blake J. 2012. Symmetry breaking cilia-driven flow in the zebrafish embryo. *J. Fluid Mech.* 705:26–45
Smith DJ. 2009. A boundary element regularized Stokeslet method applied to cilia-and flagella-driven flow. 465:3605–26
Smith DJ. 2018. Biological fluid mechanics under the microscope: a tribute to John Blake. *ANZIAM J.* 59:416–42
Smith DJ, Blake JR, Gaffney EA. 2008. Fluid mechanics of nodal flow due to embryonic primary cilia. *J. R. Soc. Interface* 5:567–73
Smith DJ, Gaffney EA, Blake JR. 2007. Discrete cilia modelling with singularity distributions: application to the embryonic node and the airway surface liquid. *B. Math. Biol.* 69:1477–510
Smith DJ, Montenegro-Johnson TD, Lopes SS. 2014. Organized chaos in Kupffer's vesicle: how a heterogeneous structure achieves consistent left-right patterning. *Bioarch.* 4:119–25

Smith DJ, Smith AA, Blake JR. 2011. Mathematical embryology: the fluid mechanics of nodal cilia. *J. Eng. Math.* 70:255–79

Sulik K, Dehart D, Inagaki T, Carson J, Vrablic T, et al. 1994. Morphogenesis of the murine node and notochordal plate. *Dev. Dyn.* 201:260–78

Supatto W, Fraser S, Vermot J. 2008. An all-optical approach for probing microscopic flows in living embryos. *Biophys. J.* 95:L29–31

Supp D, Witte D, Potter S, Brueckner M. 1997. Mutation of an axonemal dynein affects left–right asymmetry in *inversus viscerum* mice. *Nature* 389:963–66

Tabin C, Vogan K. 2003. A two-cilia model for vertebrate left-right axis specification. *Genes Dev.* 17:1–6

Takeda S, Yonekawa Y, Tanaka Y, Okada Y, Nonaka S, Hirokawa N. 1999. Left-right asymmetry and kinesin superfamily protein KIF3A: new insights in determination of laterality and mesoderm induction by *kif3A*$^{-/-}$ mice analysis. *J. Cell Biol.* 145:825–36

Tanaka Y, Okada Y, Hirokawa N. 2005. FGF-induced vesicular release of Sonic hedgehog and retinoic acid in leftward nodal flow is critical for left–right determination. *Nature* 435:172–77

Vilfan A. 2012. Generic flow profiles induced by a beating cilium. *Eur. Phys. J. E* 35:72

Wang G, Manning M, Amack J. 2012. Regional cell shape changes control form and function of Kupffer's vesicle in the zebrafish embryo. *Dev. Biol.* 370:52–62

Yoshiba S, Shiratori H, Kuo I, Kawasumi A, Shinohara K, et al. 2012. Cilia at the node of mouse embryos sense fluid flow for left-right determination via Pkd2. *Science* 338:226–31

Yuan S, Li J, Diener D, Choma M, Rosenbaum J, Sun Z. 2012. Target-of-rapamycin complex 1 (Torc1) signaling modulates cilia size and function through protein synthesis regulation. *PNAS* 109:2021–26

Yuan S, Zhao L, Brueckner M, Sun Z. 2015. Intraciliary calcium oscillations initiate vertebrate left-right asymmetry. *Curr. Biol.* 25:556–67